Deformation Mechanisms in Cr20Ni80 Alloy at Elevated Temperatures

N. R. Dudova[a], R. O. Kaibyshev[a], and V. A. Valitov[b]

[a] *Belgorod State University, ul. Pobedy 85, Belgorod, 308015 Russia*

[b] *Institute of Problems of Metal Superplasticity, Russian Academy of Sciences, ul. S. Khalturina 39, Ufa, 450001 Russia*

Abstract—The mechanisms of plastic deformation of Cr20Ni80 nichrome with an initial grain size of 80 μm were studied in the temperature range 600–950°C and the strain-rate range 1.5×10^{-6}–5×10^{-2} s^{-1}. Nichrome is shown to exhibit anomalously high values of stress exponent n and a high deformation activation energy Q. These unusual properties were found to be caused by "threshold" stresses below which deformation does not occur. An analysis of the deformation behavior with allowance for threshold stresses reveals the regions of hot, warm, and cold deformation in nichrome. At normalized strain rates $\dot{\varepsilon}kT/D_1Gb < 10^{-8}$, the true values of n and Q are ~4 and 285 ± 30 kJ/mol, respectively. In the normalized-strain range 10^{-8}–10^{-4} $n \sim 6$ and the deformation activation energy decreases to 175 ± 30 kJ/mol. This change in the deformation-behavior characteristics is explained by the transition from high-temperature dislocation climb, which is controlled by lattice self-diffusion, to low-temperature dislocation climb, which is controlled by pipe diffusion, as the temperature decreases. At $\dot{\varepsilon}kT/D_1Gb = 10^{-4}$, a power law break-down takes place and an exponential law (which describes the deformation behavior in the range of cold deformation) becomes operative.

INTRODUCTION

Superalloys based on the Ni–Cr and Ni–Fe–Cr systems are now widely used in aviation-engine turbines and electric power installations. The mechanical properties of these materials under creep conditions are practically important, since they control the service characteristics of turbines. Any increase in such parameters as the long-term creep strength and the rupture time can decrease the fuel consumption due to an increase in the operating temperature or a decrease in the weight of the parts operating at high temperatures. Modern superalloys have very high mechanical properties. A further increase in the creep strength of these alloys can only be achieved by analyzing the physical processes that occur in materials during creep.

On the other hand, a large number of superalloys are wrought materials. Detailed information on the deformation mechanisms that take place at the temperatures and strain rates of metal forming can be used to optimize technological operations and to decrease the required force in deforming tools.

Unfortunately, the deformation mechanisms that occur in them at high temperatures have been studied in a few works despite a large number of works dealing with the creep and deformation of superalloys [1]. Such creep mechanisms are poorly understood not only in complexly alloyed superalloys containing the γ′ phase or its analog with the bct lattice in Inconel-type alloys, but also in dilute Ni–Cr alloys.

It seems promising to study the deformation mechanisms in superalloys by comparing the deformation processes that occur in a γ-phase solid solution with the deformation behavior of alloys containing disperse particles [2]. The deformation mechanisms in Cr20Ni80 alloy, which has a low stacking-fault energy (SFE) [3], are analogous to the deformation mechanisms operating in the γ matrices of most superalloys. Correspondingly, detailed information on the deformation processes that proceed in nichrome is required to analyze the deformation mechanisms in superalloys containing both coherent γ′-phase particles and Y_2O_3 nanoparticles.

The available data on the deformation behavior of Cr20Ni80 alloy [1–3] were analyzed in [1] and represented in the form of deformation mechanism maps. However, these data do not yield a complete picture of the physical processes that control the strain rate. The general disadvantage of the works dealing with the deformation mechanisms in nichrome consists in insufficient structural studies. Most authors whose experimental data were summazized in [1] analyzed the mechanical properties and used the results obtained to draw conclusions concerning the deformation mechanisms operating in nichrome. Moreover, there are no data on the relation between the deformation mecha-

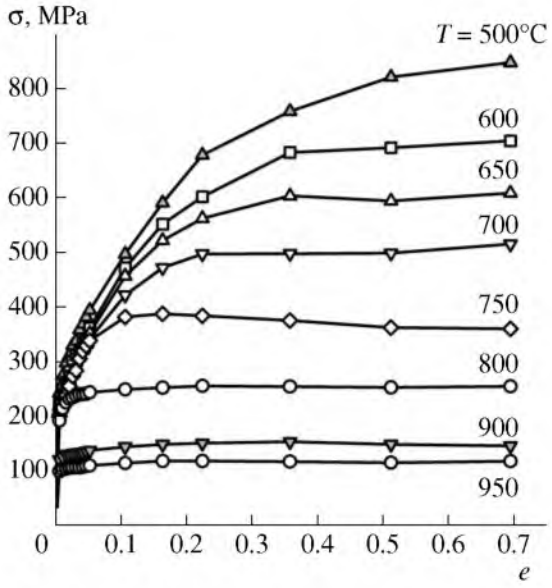

Fig. 1. True flow stresses vs. the true strain for the Cr20Ni80 alloy at a strain rate of 7×10^{-4} s^{-1} in the temperature range 500–950°C.

nisms and the structural changes during the plastic flow in Cr20Ni80 alloy.

The purpose of this work is to comprehensively analyze the plastic-deformation mechanisms in Cr20Ni80 alloy over a wide deformation-temperature range. Mechanical tests were performed according to an active loading scheme. The authors of [4] showed that the data obtained during active loading tests at a constant strain rate coincide with the data obtained during passive loading tests at a constant stress if the flow stress and the strain rate are taken at the stage of a steady-state plastic flow. Apart from the mechanical properties of nichrome, we also studied its structure. Based on a comparative analysis of the deformation behavior and electron-microscopic data, we discussed deformation mechanisms.

EXPERIMENTAL

We studied commercial Cr20Ni80 alloy (75% Ni–21% Cr–1.1% Si–0.3% Mn–0.7% Fe–0.2% Al–0.05% C) with an average grain size of 80 μm. The mechanical tests of the alloy were carried out using a Schenk universal dynamometer according to the axial compression scheme. Cylindrical 10×12-mm samples were deformed in the temperature range 500–950°C in 50°C intervals at initial strain rates ranging 1.5×10^{-6} to 5 to 10^{-2} s^{-1}. To investigate microstructural changes after high-temperature (800–950°C) tests, we rapidly cooled the samples in a water stream immediately after the termination of deformation.

To examine a deformation relief, we deposited $6 \times 5 \times 3$-mm alloy samples with preliminarily electrolytically polished lateral surfaces in a vacuum in an IMASh 20–78 vacuum device at temperatures of 500, 700, and 900°C. Slip patterns were analyzed using a JSM-840 scanning electron microscopy.

Electron-microscopic examination of the alloy was performed using a JEM-2000EX transmission electron microscope at an accelerating voltage of 160 kV. Foils were prepared by jet electrolytic polishing with a 10% solution of perchloric acid in butanol in a Struers Tenupol-3 foil preparation device.

EXPERIMENTAL RESULTS

Flow Stress–Strain Curves

In the temperature range of 500–900°C the results of mechanical tests of the Cr20Ni80 alloy demonstrate that the shape of the σ-e curves is determined by the deformation temperature (Fig. 1). At high temperature (t = 950–750°C), the flow stresses attain steady state almost instantly (at e = 0.01–0.02 and T = 900 and 800°C) or after certain hardening (at e = 0.1 and T = 750°C). The difference in the steady-state flow stresses and the yield stress $\sigma_{0.2}$ is 10–50%. At lower temperatures (600–700°C), a significant strain hardening occurs at the initial stage of plastic deformation. The flow stress at the steady-state stage, which appears at e = 0.2–0.3, is two to three times higher than the flow stress immediately after the beginning of a plastic flow. The deformation at the steady-state stage is accompanied by an insignificant monotonic increase in the stresses. It should be noted that, at $T \le 650$°C, a steady-state flow stage appears at strain rates below 10^{-3} s^{-1}. The lower the temperature, the lower the strain rate of the steady-state flow. At T = 500°C, a steady-state flow stage is not achieved even at e = 0.7. Since we failed to achieve a steady-state plastic flow at this temperature, we did not use the experimental points obtained at 500°C to analyze the deformation behavior of nichrome.

Effect of the Deformation Temperature and the Strain Rate on the Flow Stresses

To analyze the deformation behavior of the Cr20Ni80 alloy, we used the steady-state flow stress in a wide temperature–strain-rate range (T = 600–950°C, $\dot{\varepsilon} = 10^{-6}$–$10^{-2}$ s^{-1}). Apparent activation energy Q_a and the creep parameters given below were calculated using the procedures described in [4, 5].

As follows from the dependence of the strain rate on the flow stress plotted on the logarithmic scale (Fig. 2a), the experimental points fall on straight lines at any temperature in the region to the left of the dashed line (temperature range from 700 to 950°C). Therefore, the deformation behavior of nichrome in this region can be described by the power law [4–10]

$$\dot{\varepsilon} = A(\sigma/G)^n \exp(-Q/RT), \qquad (1)$$

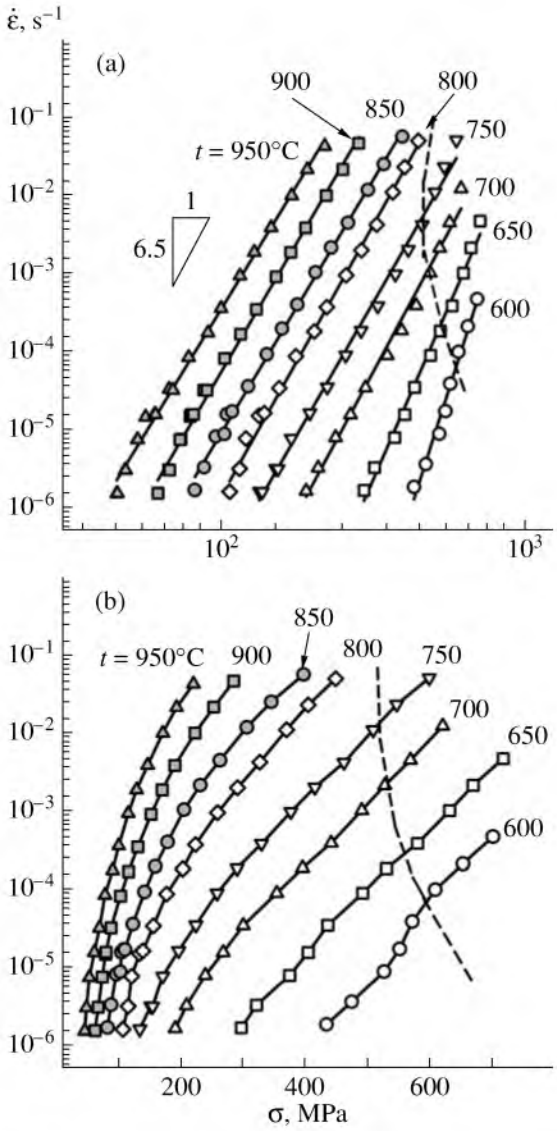

Fig. 2. Strain rate vs. the steady-state flow stress. The dashed line separates the areas of action of power and exponential laws for deformation: (a) logarithmic coordinates and (b) semilogarithmic coordinates.

where $\dot{\varepsilon}$ is the strain rate, A is a constant, n is the exponent, σ is the flow stress at the steady-state stage, G is the shear modulus, Q is the activation energy of plastic deformation, R is the gas constant, and T is the absolute temperature.

Exponent n, which is the slope of the $\log\dot{\varepsilon} - \log\sigma$ curve, increases insignificantly from 6 to 7 as the temperature decreases from 950 to 700°C. In the temperature range 800–950°C, n exhibits a weak tendency to increase with decreasing strain rate, which is a sign of "threshold" stresses [2–4]. At 650 and 600°C, the values of n are substantially higher (9 and 12, respectively). We assume that the deformation behavior of the

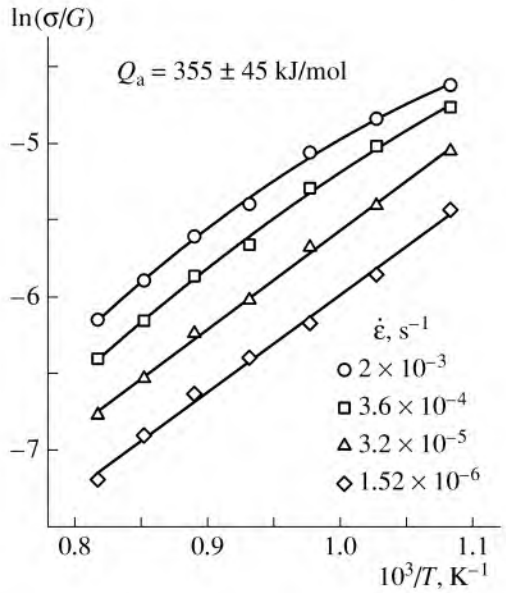

Fig. 3. Flow stresses normalized by the shear modulus vs. the reciprocal temperature.

alloy at these temperatures can be described by the exponential deformation law [6–10]

$$\dot{\varepsilon} = B\exp(\beta\sigma)\exp(-Q/RT), \qquad (2)$$

where B is a constant and β is a coefficient.

The points to the right of the dashed line fall on straight lines plotted in semilogarithmic coordinates (Fig. 2b). Hence, exponential equation (2) adequately describes the deformation behavior of the alloy at low temperatures [10].

Activation Energy of Plastic Deformation

The values of the apparent activation energy of plastic deformation Q_a were determined according to the standard procedures described in [4–6, 11–13]. Equation (1) can be algebraically converted into the equation

$$\ln(\sigma/G) = \ln(\dot{\varepsilon}/A)^{1/n} + (Q/RnT). \qquad (3)$$

The values of the apparent activation energy were calculated graphically, via plotting the stresses normalized by the shear modulus in the $\ln(\sigma/G) - 10^3/T$ coordinates at various strain rates. In the calculations, we used the shear modulus of the Ni–20% Cr alloy, which depends on the temperature as [1, 2]

$$G = 8.31 \times 10^4\{1 - 0.5[(T - 300)/1673]\}. \qquad (4)$$

Next, we determined the slope, which corresponds to $Q/(Rn)$ (Fig. 3). The values of Q_a calculated in the temperature range 950–650°C are 300–400 kJ/mol, which are significantly higher than the activation energy of lattice diffusion of Ni atoms in the Ni–20% Cr solid solution (285 kJ/mol [14]). At deformation tempera-

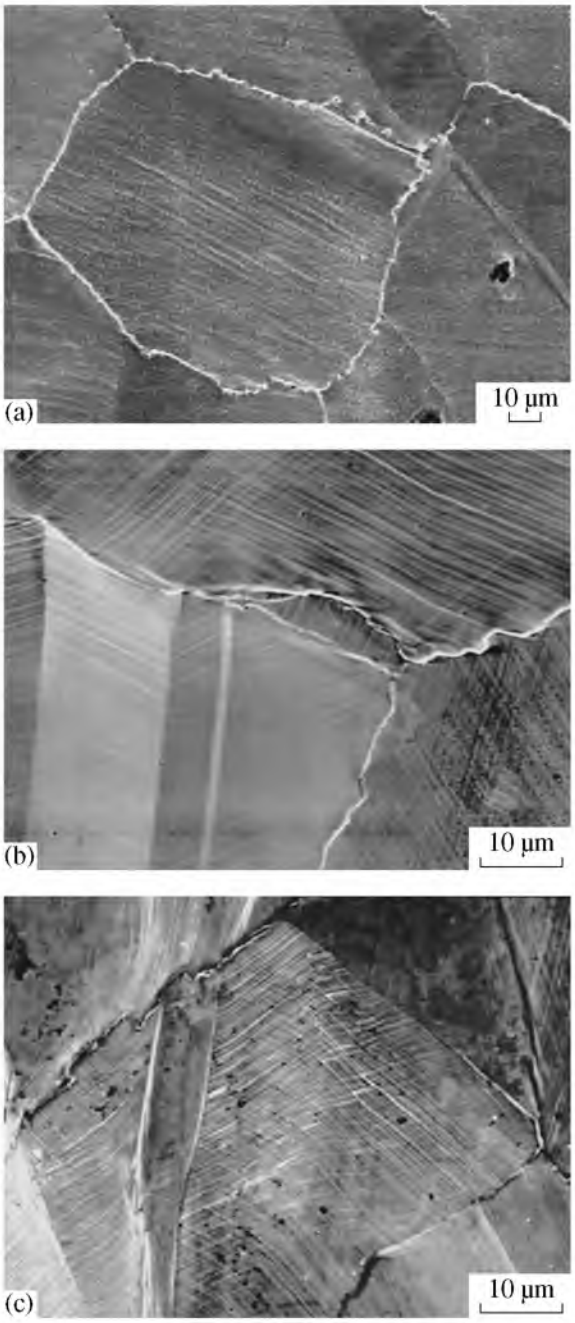

Fig. 4. Deformation relief of the Cr20Ni80 alloy deformed at a rate of $\dot{\varepsilon} = 7 \times 10^{-4}$ s^{-1}: (a) t = 900°C, e = 0.1; (b) T = 700°C, e = 0.1, and (c) T = 500°C, e = 0.17.

tures <650°C, it is impossible to calculate the activation energy with a satisfactory accuracy because of a strong increase in the exponent of the flow stress [10].

Deformation Relief

The topographic examination of the samples deformed at e = 0.1–0.17 demonstrates that the character of the crystallographic slip in the Cr20Ni80 alloy is different in different deformation-temperature ranges. In the range of high-temperature deformation (T = 900°C), the character of slip is homogeneous, without a localized plastic flow in deformation bands (Fig. 4a). One slip system is operative in most grains. In the temperature range 500–700°C, single slip is the main plastic-flow mechanism in half the quantity of grains (Figs. 4b, 4c). In the other grains, two or more slip systems are operative (Figs. 4b, 4c). The slip features are represented by long parallel lines passing through the entire grain. Rough deformation bands are observed, which indicates a strongly localized plastic flow. In some grains, slip occurs on two independent systems, and the slip lines have approximately the same contrast and intersect each other at a near-right angle. The sample surfaces have no wavy lines, which could indicate the operation of cross slip. The ability of lattice dislocations to be redistributed by cross slip is known to decrease with decreasing SFE [1, 15]. The absence of wavy traces of cross slip in the deformation relief of the Cr20Ni80 alloy, which has a low SFE, supports this rule. We can state that cross slip is not activated in nichrome even at high deformation temperatures, which facilitate the recombination of partials into perfect dislocations (which are capable of cross slip) [15, 16].

Microstructure

An analysis of the initial microstructure did not reveal nanoparticles inside the initial grains or near their boundaries (Fig. 5a). A small number of relatively large (≥1 μm) carbides was detected along certain grain boundaries. However, their number is negligibly small, and they cannot affect dislocation motion. It should be noted that the Cr20Ni80 alloy has a short-range ordering.

When studying the microstructure of the Cr20Ni80 alloy deformed at e = 1.2, we were able to distinguish three temperature ranges characterized by different microstructures (Figs. 5b–5d). In the temperature range 950–750°C, dislocations are easily redistributed, which leads to the formation of grains and subgrains more than 1 μm in size, whose volumes are free of dislocations (Fig. 5b). The presence of helical dislocations points to active dislocation climb. In the temperature range 700–650°C, dislocation climb is hindered and a mixed structure forms (Fig. 5c). The crystallite size is 0.6–0.3 μm, and a large number of lattice dislocations are present inside crystallites. The dislocation density exceeds 10^{15} m^{-2}, which results in the appearance of a specific fringe contrast and moiré patterns [18]. Dislocations are likely to travel only very short distances at these temperatures. At low temperatures (≤600°C), a low-energy dislocation structure (LEDS) typical of cold deformation forms [19]. Its formation is usually related to the dislocation climb caused by the interaction of dislocations with deformation-induced vacancies [19]. The LEDS element size is close to a nanom-

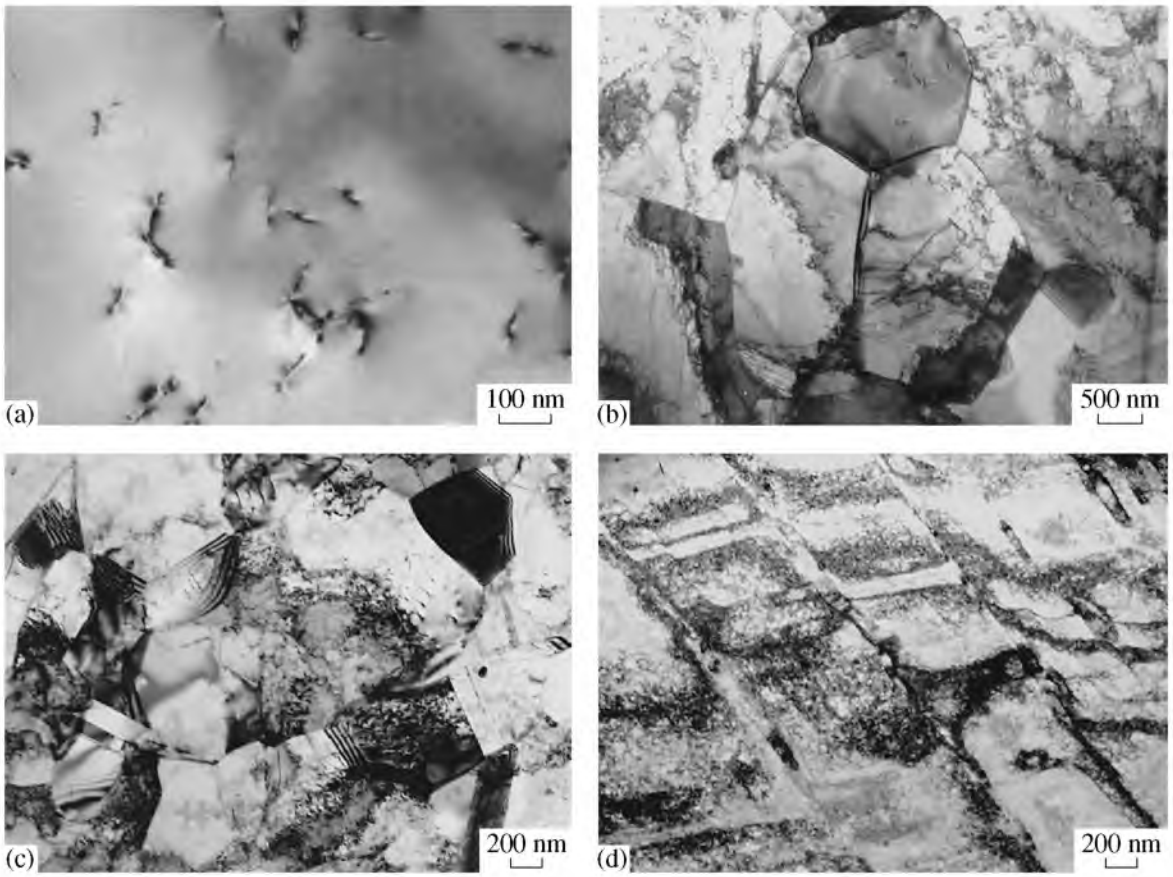

Fig. 5. Fine structure of the Cr20Ni80 alloy (a) in the initial state and after deformation at $e = 1.2$, a rate $\dot{\varepsilon} = 7 \times 10^{-4}$ s^{-1}, and a temperature T = (b) 900, (c) 700, and (d) 500°C.

eter scale (d = 170–80 nm), and the diffusion contrast at boundaries indicates a high dislocation density.

DISCUSSION OF THE RESULTS

An analysis of the deformation behavior of the Cr20Ni80 alloy suggests that this material exhibits "threshold" behavior, like materials containing disperse particles [2–4, 9, 11, 12]. This assumption is supported by the following facts. First, exponent n increases with decreasing stress at $T \geq 800$°C; second, the activation energy of plastic deformation corrected for the temperature dependence of the shear modulus exceeds the enthalpy of lattice self-diffusion. This type of deformation behavior is described in terms of threshold stresses σ_{th} [2–4, 11–13]. In this case, the strain rate at a steady-state stage is described by the equation

$$\dot{\varepsilon} = A[(\sigma - \sigma_{th})/G]^n \exp(-Q_c/RT), \qquad (5)$$

where σ is the applied stress, G is the shear modulus, n is the true exponent, Q_c is the true activation energy of plastic deformation, R is the gas constant, T is the absolute temperature, and A is a dimensionless constant. Plastic deformation is controlled by effective stresses $\sigma - \sigma_{th}$.

Threshold Stresses

To determine the threshold stresses, we used the standard procedure described in detail in [11–13]. For every temperature, the experimental data were plotted in the $\dot{\varepsilon}^{1/n} - \sigma$ coordinates, where n was taken to be 2, 3, 4, 4.5, 5, 5.5, 6, 7, and 8. If the experimental data are described by Eq. (5) and the threshold stress is constant for any temperature, the experimental points fit a

True stress exponents n and threshold stresses at various temperatures

t, °C	n	σ_{th}, MPa
600	8	220
650	7	114.8
700	6	57.6
750	6	49.5
800	5.5	45.8
850	5	40.5
900	4.5	38.5
950	4	30.8

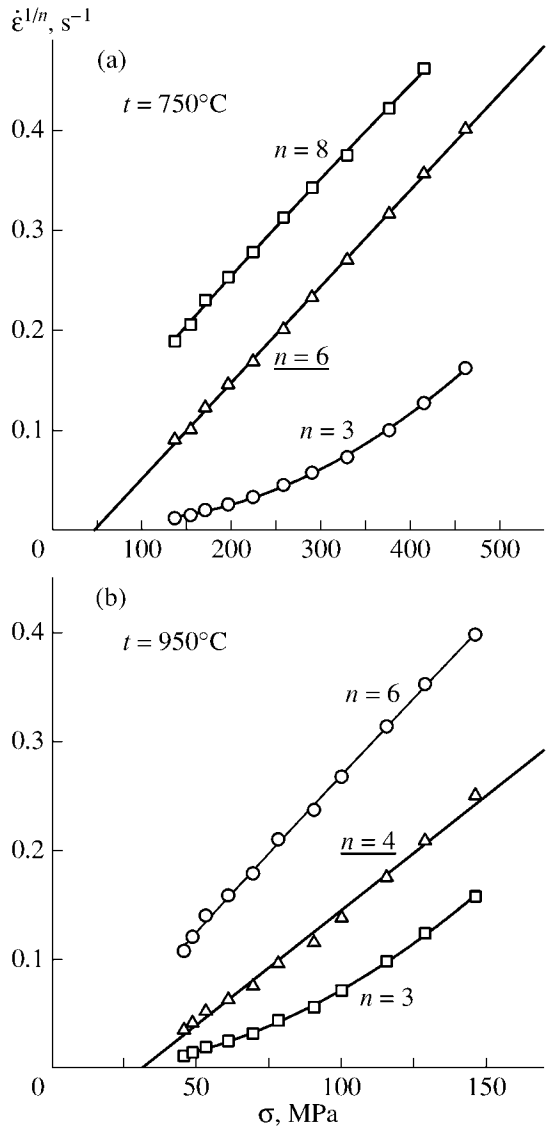

Fig. 6. $\dot{\varepsilon}^{1/n}$–σ curves for temperatures of (a) 750 and (b) 950°C. Linear approximation for determining the threshold stresses: (a) 750°C; at n = 3, the points form a concave curve; at n = 6, points fit a straight line; at n = 8, the points form a convex curve; (b) 950°C; at n = 3, the points form a concave curve; at n = 4, points fit a straight line; at n = 6, the points form a convex curve.

straight line. The value of n at which the agreement between points and the straight line is the best is taken to be the true exponent. The extrapolation of this line to $\dot{\varepsilon}^{1/n} = 0$ allows σ_{th} to be determined.

Figure 6 shows the typical $\dot{\varepsilon}^{1/n} - \sigma$ curves. At 950 and 750°C, the agreement with a straight line is the best for n = 4 and 6, respectively. At lager or smaller values of n, the experimental points form curved lines. The table gives the true exponents n and the threshold stresses for various temperatures. Stress exponent n is seen to increase from 4 to 7 as the temperature decreases from 950 to 650°C. The threshold stress decreases as the deformation temperature increases. The threshold stress is found to exceed 100 MPa at 650°C. In other words, we have every reason to believe that these threshold stresses yield the feasibility to use nichrome as a structural material at these temperatures.

The threshold stresses are described by the equation [4, 11–13]

$$\sigma_{th}/G = B_0 \exp(Q_0/RT), \qquad (6)$$

where B_0 is a constant and Q_0 is the activation energy required for a dislocation to overcome an obstacle.

Figure 7 shows normalized threshold stress σ_{th}/G as a function of the temperature in semilogarithmic coordinates. There exist two different temperature dependences of the threshold stresses that differ in the nature of threshold stresses. At 950–700°C, Q_0 is about 18.5 kJ/mol. At low temperatures (650–700°C), this value is higher (about 100 kJ/mol). At 700°C, the weak temperature dependence of the threshold stresses at high temperatures changes into the strong temperature dependence at low temperatures.

The majority of modern models consider the threshold stresses as a result of the interaction between dislocations and particles. However, these models are inapplicable to interpret our experimental data because of the absence of particles with several nanometers in size that are not dissolved upon heating. Only nanoparticles with a specific volume of ≥1% can generate the threshold stresses observed experimentally.

To explain the threshold stresses that occur during superplasticity, the authors of [20, 21] assumed that they appear as a result of the interaction of dislocations with dissolved atoms or particles less than 7 nm in size formed along grain boundaries. Note that those authors consider particles less than 7 nm in size from the standpoint of the nature of threshold stresses as clusters of dissolved atoms. Using this theory, we can explain the presence of threshold stresses in nichrome at a temperature below 700°C as the result of the interaction of dislocations with short-range ordering areas. Unfortunately, these particles can be detected by electron microscopy only using direct resolution [17]. Nevertheless, the indirect data in [22] point to the precipitation of these particles or short-range ordering in the temperature range 300–650°C. It is this short-range ordering, which is responsible for the Portevin–Le Chatelier effect and a positive temperature dependence of the flow stresses in nichrome at these temperatures [22], that can cause the high values of threshold stress and, correspondingly, can ensure a satisfactory creep strength of nichrome. This assumption is supported by the data in [23–25], where coherent $Al_3(Sc, X)$ particles 5–30 nm in size were shown to provide high threshold stresses.

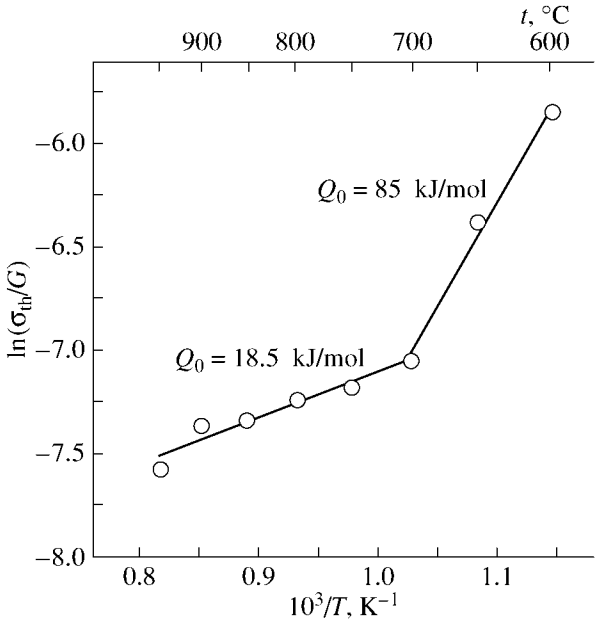

Fig. 7. Normalized threshold stresses vs. the reciprocal temperature in semilogarithmic coordinates.

The nature of the threshold stresses at temperatures ≥700°C is unclear. We can only assume that the threshold stresses can result from barriers similar to Lomer–Cottrell barriers, which form upon the intersection of moving dislocations belonging to different systems. As the deformation temperature increases, predominantly multiple slip changes into predominantly single slip; as a result, the probability of dislocation intersection decreases, which decreases the threshold stresses.

True Activation Energy of Plastic Deformation

To determine the true activation energy of plastic deformation, we plotted the dependence of the normalized effective stresses against the reciprocal temperature in semilogarithmic scales (Fig. 8a). There are two temperature ranges (650–700°C, 700–950°C) having different slopes k. It should be noted that the shapes of these curves very weakly change with the strain rate, which indicates a high accuracy in determining the threshold stresses.

Figure 8b shows the variation of the true activation energy of plastic deformation; at 950–750°C, this energy is seen to be 285 ± 30 kJ/mol, which corresponds to the activation energy of lattice diffusion of nickel atoms in a Ni–20% Cr solid solution (285 kJ/mol) [14]. At 700 and 650°C, the activation energy is 175 ± 30 kJ/mol, which corresponds to the activation energy of pipe diffusion of nickel atoms in a Ni–20% Cr solid solution (170 kJ/mol) [14]. The increase in the activation energy of plastic deformation with the deformation temperature can be explained by the transition from low-temperature dislocation climb

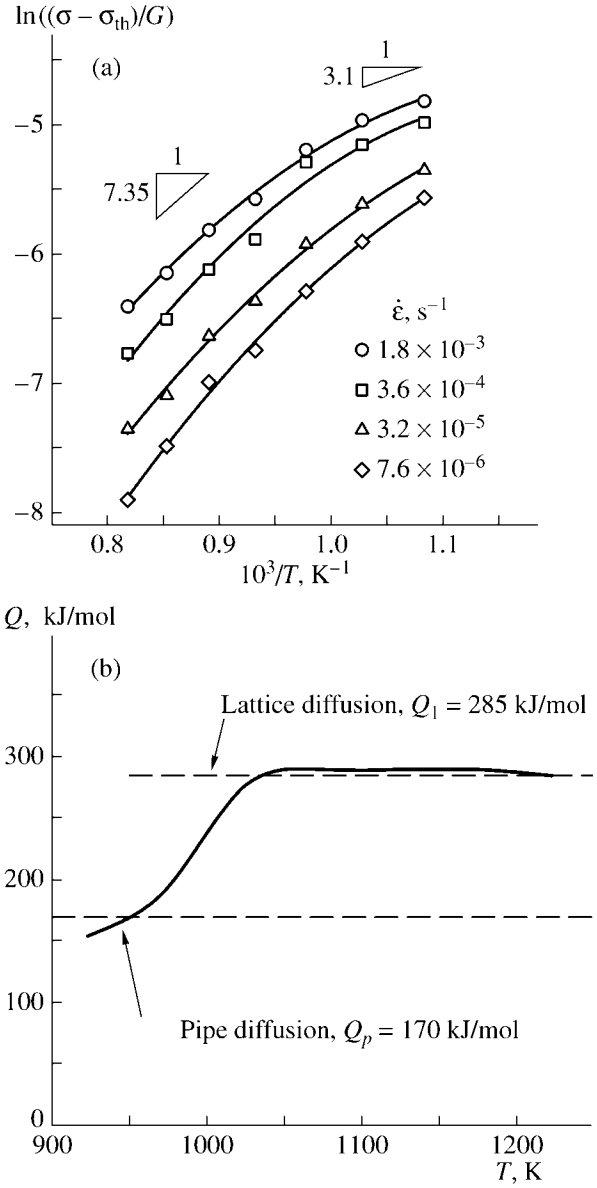

Fig. 8. (a) Normalized effective stresses vs. the reciprocal temperature in semilogarithmic coordinates and (b) the variation of the true activation energy of plastic deformation with the temperature.

controlled by pipe diffusion to high-temperature dislocation climb controlled by lattice diffusion [6, 7, 11, 12]. Since the studies of the deformation relief revealed no signs of cross slip, we have every reason to believe that dislocations in nichrome are redistributed only via climb. As a result, a decrease in the dislocation climb rate strongly affects the deformation behavior of such materials and structural changes in them. The transition from rapid high-temperature to slow low-temperature climb leads to a sharp increase in the density of lattice dislocations and a decrease in the size of the forming structural elements. We assume that the sizes of the grains and/or subgrains forming in the hot- or warm-

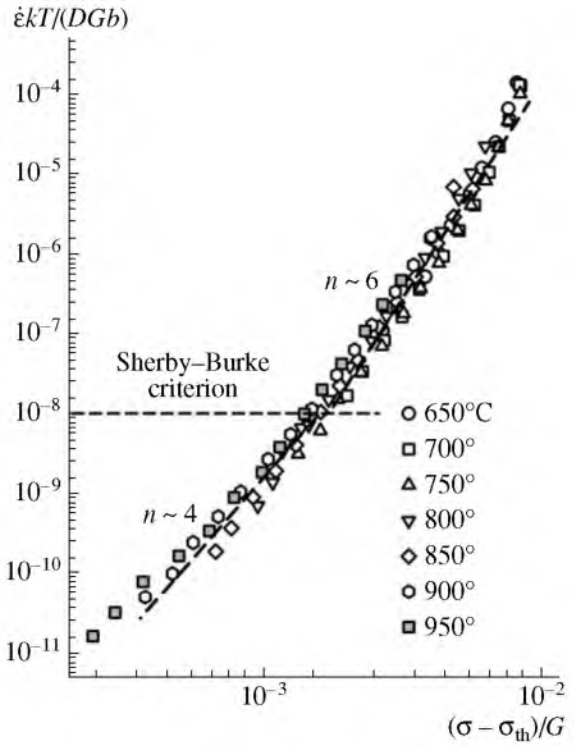

Fig. 9. Normalized strain rates vs. the normalized effective stresses.

deformation region are controlled by dislocation climb path.

Temperature Dependence of the Normalized Strain Rate on the Reduced Flow Stresses

Figure 9 shows the dependence of the normalized strain rate $\dot{\varepsilon}$ on the normalized effective stresses σ–σ_{th} obtained for the Cr20Ni80 alloy. For the normalization, we used the temperature dependences of the shear modulus (Eq. (4)) and the lattice diffusion coefficient of nickel atoms in a Ni–20% Cr solid solution [14]:

$$D_1 = D_0 \exp(-Q_1/RT), \qquad (7)$$

where $D_0 = 1.6 \times 10^{-4}$ m^2 s^{-1} is the preexponential factor and $Q_1 = 285$ kJ/mol is the activation energy of lattice diffusion of nickel atoms in a Ni–20% Cr solid solution. The Burgers vector is $b = 2.5 \times 10^{-10}$ m [1].

It is seen that the Cr20Ni80 alloy exhibits two characteristic types of deformation behavior, which differ in the character of the flow-stress dependence of the strain rate. In the hot-deformation region (located at low normalized strain rates ($<10^{-8}$) and high temperatures (t = 950–750°C)), a power law with the stress exponent $n \sim 4$ is valid. Allowing for the true activation energy of deformation, we can relate this deformation behavior to high-temperature dislocation climb controlled by lattice self-diffusion.

The warm-deformation region is located at average normalized strain rates (10^{-8}– 10^{-4}), where the slope of the linear dependence is $n \sim 6$. For this transition, the classical relation $n_{lt} = n_{ht} + 2$ is valid [6–10]. The points lying on the straight-line section with a slope of 6 fall in the stress range where the true activation energy of deformation approaches the activation energy of pipe diffusion. This transition can be explained using the terms employed to explain the variation of the true activation energy of plastic deformation. The transition from rapid high-temperature dislocation climb to slow low-temperature dislocation climb decreases the dislocation climb rate, which correlates with the results of structural studies.

The inflection point corresponding to the normalized rate $\dot{\varepsilon}\, kT/(D_1Gb) = 10^{-8}$ is a clear boundary between the hot- and warm-deformation regions for the Cr20Ni80 alloy. This inflection point coincides with the Sherby–Burke criterion [26], although this criterion should separate a warm-deformation from a cold-deformation region, in which the deformation behavior of materials is described by exponential law (2). A similar result was obtained in [11–13], where the deformation behavior of materials was also analyzed in terms of threshold stresses. The region of a power law changes into the region of an exponential law at a normalized rate of about 10^{-4} and a temperature of about 600°C. Thus, the power law is violated at a rate that is four orders of magnitude higher than the rate corresponding to the Sherby–Burke criterion ($\dot{\varepsilon}\, kT/(D_1Gb) = 10^{-8}$). The transition from the warm-deformation to the cold-deformation region is unambiguously supported by the results of studying the fine structure of nichrome. The Sherby–Burke criterion is likely to separate the temperature–rate region in which dislocations can travel significant distances, which makes it possible to maintain an unchanged density of individual lattice dislocations at the steady-state flow due to both dislocation annihilation and dislocation arrangement into subgrain boundaries and/or dislocation adsorption by the high-angle boundaries of deformation-induced grains. In the temperature–rate region lying above the Sherby–Burke criterion, the dislocation density can decrease during the steady-state flow mainly due to dislocation annihilation. This causes the increase in the density of lattice dislocations in nichrome by several orders of magnitude during the transition from hot to warm deformation. As a result, a steady-state flow in the region of warm deformation is achieved at significantly higher strains than in the region of hot deformation. In the region of cold deformation, the impossibility of cross slip strongly restricts dislocation redistribution, which results in dislocation annihilation. Correspondingly, it is difficult to achieve a steady-state flow, where the number of dislocations generated by sources must be equal to the number of lattice dislocations that disappear from the bulk of crystallites.

CONCLUSIONS

We studied the deformation behavior of a coarse-grained Cr20Ni80 alloy in the temperature range 600–950°C and the strain-rate range 1.5×10^{-6}–5×10^{-2} s^{-1} and showed that it exhibits "threshold" behavior similarly to precipitation-strengthened alloys. The threshold stresses were found to be ~115 MPa at 650°C and ~200 MPa at 600°C. These threshold stresses ensure the high creep strength characteristics of nichrome at these temperatures. An increase in the temperature leads to a decrease in the threshold stresses. We revealed two ranges in the temperature dependence of the threshold stresses that have different activation energies Q_0 required for a dislocation to overcome an obstacle. At 950–700°C and 650–700°C, the values of Q_0 are approximately 18.5 and 100 kJ/mol, respectively.

Using the term threshold stresses, we were able to determine two temperature ranges in the area of operation of a power law, namely, a hot-deformation range with a true stress exponent of $n \sim 4$ and a warm-deformation range with $n \sim 6$. The transition between these two ranges is located at a normalized strain rate $\dot{\varepsilon} kT/D_1Gb = 10^{-8}$, which coincides with the Sherby–Burke criterion. The transition to the area of action of an exponential law for plastic deformation occurs at a normalized rate of $\sim 10^{-4}$ and a temperature of ~600°C. We analyzed the deformation behavior of nichrome in terms of threshold stresses and found that the true activation energy of plastic deformation decreases from 285 ± 30 kJ/mol, which corresponds to high temperatures (950–750°C), to 175 ± 30 kJ/mol at low temperatures (700–650°C). This deformation behavior can be related to the transition from high-temperature dislocation climb, which is controlled by lattice self-diffusion, to low-temperature dislocation climb, which is controlled by pipe diffusion.

The distinguished temperature ranges were shown to be characterized by specific structural changes. The mechanical behavior of the Cr20Ni80 alloy, the deformation mechanisms, and the forming dislocation structure were found to be correlated.

ACKNOWLEDGMENTS

We thank M.Kh. Mukhametrakhimov for his assistance in the experimental work.

This work was supported by INTAS, project no. 2001/1-49.

REFERENCES

1. H. J. Frost and M. F. Eshby, Deformation-Mechanism Maps (Pergamon, Oxford, 1982; Metallurgiya, Chelyabinsk, 1989).
2. R. W. Lund and W. D. Nix, "High Temperature Creep of Ni–20Cr–2ThO_2 Single Crystals," Acta Metall. **24**, 469–478 (1976).
3. W. C. Oliver and W. D. Nix, "High Temperature Deformation of Oxide Dispersion Strengthened Al and Al–Mg Solid Solutions," Acta Metall. **30**, 1335–1347 (1982).
4. Y. Li, S. R. Nutt and F. Mohamed, "An Investigation of Creep and Substructure Formation in 2124 Alloy," Acta Mater. **45**, 2607–2620 (1997).
5. R. Pickens, T. J. Langan, R. O. England, and M. A. Liebson, "Study of the Hot Working Behavior of SiC–Al Alloy Composites and Their Matrix Alloys by Hot Torsion Testing," Metall. Trans. A **18** (2), 303–312 (1987).
6. S. Raj and T. Langdon, "Creep Behavior of Copper at Intermediate Temperatures: I. Mechanical Characteristics," Acta Metall. **37** (2), 843–852 (1989).
7. H. Luthy, A. Miller, and O. Sherby, "The Stress and Temperature Dependence of Steady State Flow at Intermediate Temperature for Pure Polycrystalline Aluminum," Acta Metall. **28** (2), 169–182 (1980).
8. J.-P. Poirier, *Creep of Crystals. High-Temperature Deformation Processes in Metals, Ceramics and Minerals* (Cambridge University Press, Cambridge, 1985; Mir, Moscow, 1987).
9. J. Čadek, *Creep in Metallic Materials* (Elsevier, Amsterdam, 1988; Academia, Praque, 1994).
10. M. R. Drury and F. J. Humphreys, "The Development of Microstructure in Al–5% Mg during High Temperature Deformation," Acta Metall. **34**, 2259–2271 (1986).
11. R. Kaibyshev, O. Sitdikov, I. Mazurina, and D. R. Lesuer, "Deformation Behavior of a 2219 Al Alloy," Mater. Sci. Eng., A **334**, 104–113 (2002).
12. R. Kaibyshev, F. Musin, E. Avtokratova, and Y. Motohashi, "Deformation Behavior of a Modified 5083 Aluminum Alloy," Mater. Sci. Eng., A **392** (1–2), 373–379 (2005).
13. R. Kaibyshev and I. Kazakulov, "Deformation Behavior of Fe–3% Si Steel," Mater. Sci. Techn. **20** (2), 221–228 (2004).
14. *Numerical Data and Functional Relationships in Science and Technology*, Landolt–Börnshtein, New series, Group III, Vol. 26: Crystals and Solid State Physics, Diffusion in Solid Metals and Alloys (Springer, Berlin, 1990).
15. W. Püschl, "Models for Dislocation Cross-Slip in Close-Packed Crystal Structures: A Critical Review," Prog. Mater. Sci. **47** (4), 415–461 (2002).
16. J. Fridel, *Dislocations* (Pergamon, Oxford, 1964; Mir, Moscow, 1967).
17. A. Arya, G. K. Dey, V. K. Vasudevan, and S. Banerjee, "Effect of Chromium Addition on the Ordering Behavior of Ni–Mo Alloy: Experimental Results vs. Electronic Structure Calculations," Acta Mater. **50**, 3301–3315 (2002).
18. A. Galiyev and R. Kaibyshev, "Microstructural Evolution in ZK60 Magnesium Alloy during Severe Plastic Deformation," Mater. Trans. **42** (7), 1190–1199 (2001).
19. B. Bay, N. Hansen, D. A. Hughes, and D. Kuhlmann-Wilsdorf, "Evolution of FCC Deformation Structures in Polyslip," Acta Mater. **40**, 205–219 (1992).
20. S. Yan, J. C. Earthman, and F. A. Mohamed, "Effect of Cd on Superplastic Flow in the Pb–62 wt % Sn Eutectic," Philos. Mag. A **69**, 1017–1038 (1994).

21. F. A. Mohamed, "On the Origin of Superplastic Flow at Very Low Stresses," Mater. Sci. Eng., A **410–411** (25), 89–94 (2005).
22. N. R. Dudova, R. O. Kaibyshev, and V. A. Valitov, "Manifestation of the Portevin–Le Chatelier Effect in the Kh20N80 Alloy," Fiz. Met. Metalloved. **105** (1), 105–112 (2008) [Phys. Met. Metallogr. **105** (1), 98–105 (2008)].
23. D. N. Seidman, E. A. Marquis, and D. C. Dunand, "Precipitation Strengthening at Ambient and Elevated Temperatures of Heat-Treatable Al(Sc) Alloys," Acta Mater. **50**, 4021–4035 (2002).
24. E. A. Marquis, D. N. Seidman, and D. C. Dunand, "Precipitation Strengthening at Ambient and Elevated Temperatures of Heat-Treatable Al(Sc) Alloys (Comments)," Acta Mater. **51**, 285–287 (2003).
25. E. Marsha, D. C. Dunand, van Dalen, and D. N. Seidman, "Effects of Ti Additions on the Nanostructure and Creep Properties of Precipitation-Strengthened Al–Sc Alloys," Acta Mater. **53** (15), 4225–4235 (2005).
26. O. D. Sherby and P. M. Burke, "Mechanical Behavior of Crystalline Solids at Elevated Temperature," Prog. Mater. Sci. **13**, 325–390 (1967).